

1 **Performance of the Global Forecast System’s Medium-Range**  
2 **Precipitation Forecasts in the Niger River Basin Using Multiple**  
3 **Satellite-Based Products**

4 Haowen Yue<sup>1</sup>, Mekonnen Gebremichael<sup>1</sup>, and Vahid Nourani<sup>2</sup>

5 <sup>1</sup> Department of Civil and Environmental Engineering, University of California, Los Angeles, CA 90095-1593

6 <sup>2</sup> Faculty of Civil Engineering, University of Tabriz, Tabriz, Iran

7

8

9 *Correspondence to:* Mekonnen Gebremichael ([mekonnen@seas.ucla.edu](mailto:mekonnen@seas.ucla.edu))

10

11 **Abstract.** Accurate weather forecast information has the potential to improve water resources management, energy,  
12 and agriculture. This study evaluates the accuracy of medium-range (1 – 15 day) precipitation forecasts from the  
13 Global Forecast System (GFS) over watersheds of eight major dams (Selingue Dam, Markala Dam, Goronyo Dam,  
14 Bakolori Dam, Kainji Dam, Jebba Dam, Dadin Kowa Dam, and Lagdo Dam) in the Niger river basin using NASA’s  
15 Integrated Multi-satellitE Retrievals (IMERG) “Final Run” satellite-gauge merged rainfall observations. The results  
16 indicate that the accuracy of GFS forecast varies depending on climatic regime, lead time, accumulation timescale,  
17 and spatial scale. The GFS forecast has large overestimation bias in the Guinea region of the basin (wet climatic  
18 regime), moderate overestimation bias in the Savannah region (moderately wet climatic regime), but has no bias in  
19 the Sahel region (dry climate). Averaging the forecasts at coarser spatial scales leads to increased forecast accuracy.  
20 For daily rainfall forecasts, the performance of GFS is very low for almost all watersheds except for Markala and  
21 Kainji dams, both of which have much larger watershed areas compared to the other watersheds. Averaging the  
22 forecasts at longer time scales also leads to increased forecast accuracy. The GFS forecasts, at 15-day accumulation  
23 timescale, have better performance, but tend to overestimate high rain rates. Additionally, the performance assessment  
24 of two other satellite products was conducted using IMERG Final estimates as reference. The Climate Hazards Group  
25 InfraRed Precipitation with Station data (CHIRPS) satellite-gauge merged product has similar rainfall characteristics  
26 with IMERG Final, indicating the robustness of IMERG Final. The IMERG “Early Run” satellite-only rainfall product  
27 is biased in the dry Sahel region, however in the wet Guinea and Savannah regions, IMERG “Early Run” outperforms  
28 GFS in terms of bias. We recommend exploring appropriate post-processing calibration techniques that use near-real  
29 time products, such as, IMERG Early, to improve the performance of GFS in the wet regions, particularly at shorter  
30 time scales.

31

32

## 33 1. Introduction

34 Global climate forecasts, with lead times ranging from hours to several months, are becoming increasingly available  
35 (Saha et al. 2014; Abdalla et al. 2013; NCEP 2015; JMA 2019). Significant societal benefit could be realized from  
36 research to reduce common barriers in climate forecast utilization blocking the path to improving water resources  
37 management, energy, and agriculture. One such a barrier is the lack of understanding of climate forecast accuracy in  
38 different regions of the world. This focus is timely given the recent advances in numerical atmospheric models, and  
39 in the wealth of new observing capabilities including satellite remote sensing. These combined models and  
40 observational datasets provide opportunity for researchers to quantify the accuracy of climate forecasts.

41  
42 The Niger River is the principal river of West Africa, and is shared among nine riparian countries (Fig. 1): Benin,  
43 Burkina Faso, Cameroon, Chad, Guinea, Ivory Coast, Mali, Niger and Nigeria. The basin is facing multiple pressures  
44 from increasing population, water abstraction for irrigation, and risk of extreme hydrological events due to climate  
45 change (Sylla et al. 2018). A number of hydropower dams exist in the region, and additional dam projects are  
46 envisaged in order to alleviate chronic power shortages in the countries of the Niger basin. Optimal management of  
47 water resources is key to maximizing benefits, such as hydropower generation, and minimize disasters, such as  
48 flooding. Climate forecast information has the potential to improve water resources management, energy, and  
49 agriculture (e.g., Patt et al. 2007; Breuer et al. 2010; Mase and Prokopy 2014; Pandya et al. 2015; Koppa et al. 2019;  
50 Alexander et al. 2020). For example, in a recent study, Koppa et al (2019) showed that the use of seasonal precipitation  
51 forecasts in reservoir planning of Omo Gibe dam in Ethiopia can increase annual hydropower generation by around  
52 40%.

53  
54 Several studies have investigated the accuracy of seasonal forecasts in West Africa (e.g., Bliefert et al. 2019;  
55 Pirret et al. 2020). Seasonal forecasts are important for water resource planning, while medium-range (1-day to 15-  
56 day) forecasts are important for operational decisions, such as reservoir operations. The availability of medium-range  
57 global climate forecasts has grown in recent years. Examples of such forecast products include Global Forecast System  
58 (GFS; NCEP 2015), NCEP climate forecast system (NSF CFS, Saha et al. 2014), European Centre for Medium-Range  
59 Weather Forecasts (ECMWF; Abdalla et al. 2013), and Global Spectral Model (GSM; JMA 2019). For these  
60 precipitation forecasts to be effectively used in applications, their accuracy must be known, which is usually performed

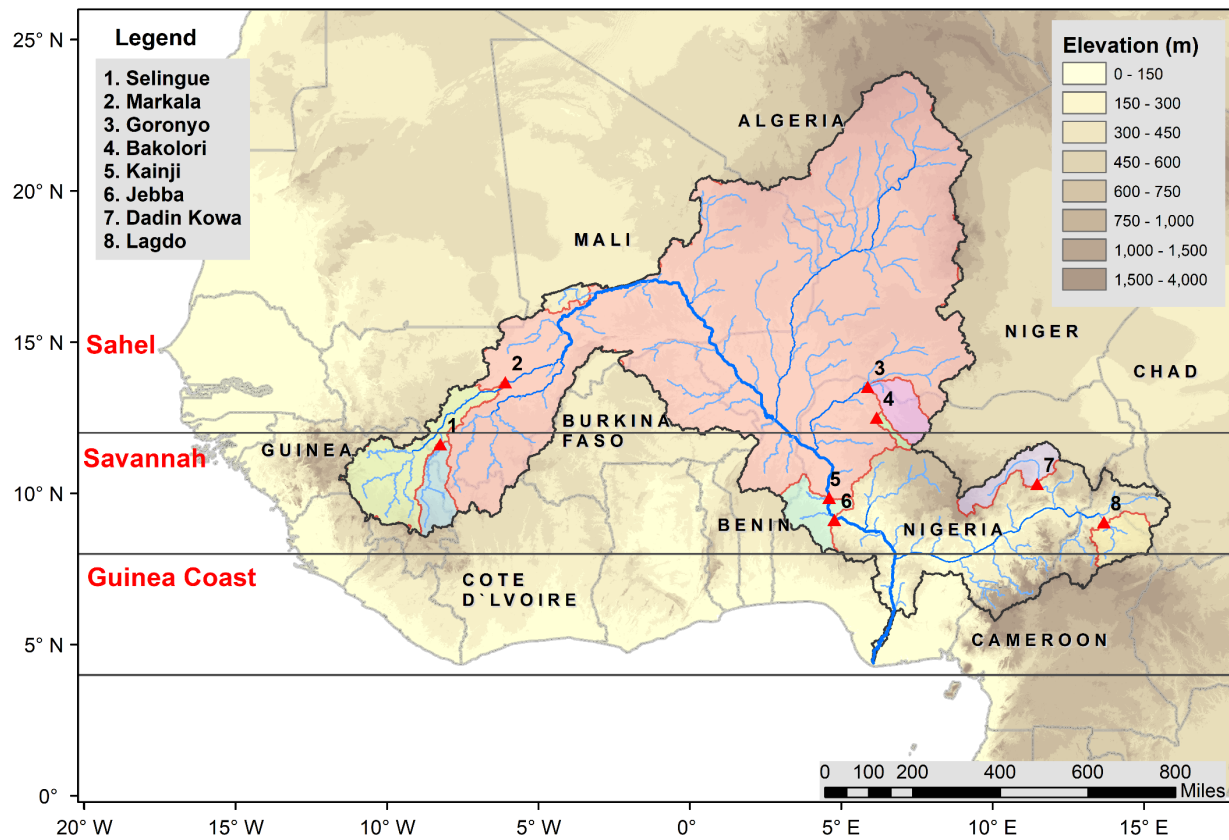


Figure 1. The Niger River Basin, and locations of major reservoir dams in the basin: (1) Selingue, (2) Markala, (3) Goronyo, (4) Bakolori, (5) Kainji, (6) Jebba, (7) Dadin Kowa, and (8) Lagdo.

61 through comparison of precipitation forecasts to observations (e.g., Tian et al. 2017; Yuan et al. 2014). Wang et al.  
 62 (2019) performed numerical experiment to examine the sensitivity of GFS to inclusion or exclusion of additional  
 63 observations collected over the eastern Pacific during the El Niño Rapid Response (ENRR) field campaign, type of  
 64 data assimilation method to prepare the initial conditions, and inclusion or exclusion of stochastic parameterizations  
 65 in the forecast model. They reported that the GFS forecast errors are only slightly sensitive to the additional ENRR  
 66 observations, more sensitive to the DA methods, and most sensitive to the inclusion of stochastic parameterizations in  
 67 the model. In addition, they reported that GFS forecasts have difficulty to capture the location and magnitude of heavy  
 68 rain rates. Sridevi et al. (2018) evaluated the performance of GFS in India by using rain gauge and satellite rainfall  
 69 product, and reported that the GFS forecast shows some skills in 1-day and 2-day lead times, but low skills from 3-  
 70 day onwards. Lien et al. (2016) compared the statistical properties of GFS forecasts and Tropical Rainfall Measuring  
 71 Mission (TRMM) Multisatellite Precipitation Analysis (TMPA; Huffman et al. 2007, 2010) observations. They  
 72 reported that the GFS model has positive bias in precipitation amount compared to TMPA observations, and that the

73 GFS forecasts have large random errors at higher resolutions, especially for convective precipitation. According to  
74 Jiang et al. (2015) the lack of consideration of the Aerosol-Cloud Interactions (ACIs) in the GFS model leads to  
75 significant bias in the GFS precipitation forecasts.

76

77 In our study region of the Niger River basin, there has not been any performance evaluation of GFS precipitation  
78 forecasts to date. The Niger basin lies in three different climate regimes (wet regime, moderately wet regime, and dry  
79 regime), and is home to nine major irrigation and hydropower dams (Selingue, Markala, Goronyo, Bakolori, Kainji,  
80 Jebba, Dadin Kowa, and Lagdo). Recent advances in satellite rainfall products, particularly following the Global  
81 Satellite Measurement satellite mission (GPM; Hou et al. 2014), and extensive evaluation of GPM rainfall products  
82 in West Africa, provides us with opportunity to use GPM rainfall products as reference for evaluation. Many studies  
83 have conducted to evaluate the accuracy of the satellite rainfall estimates in West Africa. Dezfuli et al. (2017a)  
84 evaluated the performance of NASA's Integrated Multi-satellitE Retrievals (IMERG) "Final Run" (IMERG Final)  
85 (version 4; Huffman et al. 2019a, b) in comparison with two, high-resolution, experimental rain gauge station data  
86 provided by the Trans-African Hydro-Meteorological Observatory (TAHMO; van de Giesen et al. 2014), and reported  
87 the capability of IMERG Final to represent well the diurnal cycle of rainfall. Using the same dataset, Dezfuli et al.  
88 (2017b) showed that IMERG Final is able to capture the propagation of large Mesoscale Convective Systems (MCSs),  
89 a significant advantage over its predecessor's (TMPA) 3-hourly temporal resolution, which misses the time evolution  
90 of most of these systems. Gossett et al. (2018) evaluated the performance of a number of satellite rainfall products  
91 (focusing only on versions that do not include rain gauge data) by comparison with rain gauge station networks in  
92 Benin and Niger, and reported that the satellite products (especially IMERG Early) exhibit high performance in Niger  
93 but relatively lower performance in Benin. Satgé et al. (2020) evaluated the accuracy of a number of gridded  
94 precipitation datasets over West Africa through comparison against rain gauge station data, and reported that CHIRPS  
95 and TMPA (the predecessor to IMERG) provided reliable estimates at both daily and monthly timescales, while the  
96 remaining satellite products considered (CMORPH, PERSIANN, GSMaP, ARC, and TAMSAT) and all atmospheric  
97 reanalysis products considered (MERRA and JRA) were deemed unreliable. Furthermore, they found out that satellite  
98 products that incorporated rain gauge information outperformed satellite-only products. Maranan et al. (2020)  
99 compared IMERG Final products against experimental rain gauge station data in the moist forest region of Ghana,

100 West Africa, and showed that IMERG Final datasets are able to capture monthly rainfall with a correlation coefficient  
101 close to unity.

102  
103 The objective of this study is to evaluate the accuracy of medium-range precipitation forecasts derived from the Global  
104 Forecast System (GFS) for the major reservoir dams of the Niger basin through comparison against IMERG Final.  
105 We chose GFS model due to its relatively high spatial ( $0.25^\circ \times 0.25^\circ$ ) and temporal resolution (3-hourly to 6-hourly)  
106 as well as free-of-charge data availability to users. The main questions addressed in this study are as follows. First,  
107 how does the accuracy of GFS forecast vary across different reservoir dams in the same basin? Second, how does the  
108 accuracy vary with lead time in the range 1- to 15-day? Third, what is the effect of spatial averaging (from  $0.25^\circ$  all  
109 the way to basin-scale) and temporal aggregation (from 1-day to 15-day) on the forecast accuracy? Fourth, how does  
110 the accuracy of GFS forecast compare with the accuracy of satellite-only rainfall products that are available in near-  
111 real-time, as the latter may have the potential to calibrate and improve the accuracy of GFS?

112

## 113 **2. Data and Methodology**

### 114 **2.1 Global Forecast System (GFS) Medium-Range Precipitation Forecasts**

115  
116 The Global Forecast System (GFS) is a global numerical weather prediction system run by the U.S. National Weather  
117 Service (NWS). The GFS forecast products with a resolution of  $0.25^\circ$  by  $0.25^\circ$  are obtained from National Center for  
118 Atmospheric Research (NCAR) Research Data Archive (RDA) GFS Historical Archive (NCEP 2015). The GFS is  
119 run four times a day at UTC 00, UTC 06, UTC 12, and UTC 18 hours. One of the GFS model output variables is  
120 accumulated precipitation, where the precipitation forecasts are accumulations starting from the model run time. We  
121 obtained the 1-day lead daily rainfall forecast by subtracting the 24-hour rainfall accumulation forecast from the 48-  
122 hour rainfall accumulation forecast. Similarly, in order to obtain the 5-day lead daily rainfall forecast, we subtracted  
123 the 120-hour rainfall accumulation forecast from the 144-hour rainfall forecast. We only considered the model runs at  
124 UTC 00 hour.

125  
126 The GFS model went through a major upgrade, and its version-15 forecasts are available since June 12, 2019. In  
127 version 15, the Finite Volume Cubed Sphere dynamical model (FV3) replaced the Global Spectral Model (GSM) as

128 the core model. In the GSM model, the horizontal resolutions were T1543 (12.5km) from 0 to 240 hours (0-10 days)  
129 and T574 (~34km) from 240 to 384 hours (10-16 days) (NCEP 2021a). However, in the FV3 model, the horizontal  
130 resolution of the model is about 13 km for days 0-16 (NCEP 2021b). The model runs are re-gridded to produce  
131 precipitation forecasts at 0.25° resolution (NCEP 2015). The Key FV3 model schemes include (Putman and Lin 2007):  
132 (1) the Rapid Radiative Transfer Method for GCMs (RRTMG) scheme for shortwave/longwave radiation (Mlawer et  
133 al. 1997; Iacono et al. 2000; Clough et al. 2005), (2) the Hybrid eddy-diffusivity mass-flux (EDMF) scheme for  
134 Planetary Boundary Layer (PBL) (NCEP, 2021a), (3) the Noah Land Surface Model (LSM) scheme for land surface  
135 option (Chen et al. 1997), (4) the Simplified Arakawa-Schubert (SAS) deep convection for cumulus parameterization  
136 (Arakawa et al. 1974; Grell 1993), and (5) an advanced GFDL microphysics scheme for microphysics (NCEP, 2021b).

137

## 138 **2.2 IMERG Final Satellite Precipitation Products**

139 IMERG Final rainfall products are used in this study as reference to evaluate the performance of GFS precipitation  
140 forecasts. IMERG Final combines all available microwave precipitation estimates, microwave-calibrated infrared  
141 estimates, and rain gauge data to provide rainfall estimates at very high resolution (30-minute, 0.10°) (Hou et al. 2014;  
142 Huffman et al. 2015). The IMERG products are categorized into three types, namely early run, late run, and final run.  
143 It is only the final run or “final” version that incorporates rain gauge data. The data latency of IMERG Final is about  
144 3.5 months. Details of IMERG algorithm developed by NASA are available at Huffman et al (2019a, b). The latest  
145 version (V6B) of IMERG datasets have been accessed from the NASA’s Earth Data Goddard Earth Sciences Data  
146 and Information Services Center (GES DISC) web portal.

147

## 148 **2.3 Other Satellite Precipitation Products**

149 In order to put the GFS forecast performance into perspective, we also evaluated two other state-of-the-art satellite  
150 rainfall products:

- 151 • IMERG Early provides un-calibrated IMERG rainfall fields, which do not include correction from rain gauges.  
152 The data latency of IMERG Early is near-real-time, about 4 hours. We have used the latest version (V6B) of  
153 IMERG Early datasets. Post-processing calibration of GFS forecasts (in order to improve the accuracy of GFS  
154 forecasts) requires the use of “relatively better performing” and “available in near-real-time” independent  
155 rainfall observations to correct real-time dynamical GFS model forecasts. Comparison of the performance of

156 IMERG Early with the performance of GFS would indicate to what extent the IMERG Early products could be  
157 used for calibration of GFS forecasts.

158 • The Climate Hazards Group InfraRed Precipitation with Station data (CHIRPS) is derived primarily from  
159 thermal infrared data using the cold cloud duration (CCD) approach, calibrated using TRMM Multi-satellite  
160 Precipitation analysis (TMPA 3B42 v7; Huffman et al. 2007) precipitation datasets by local regression, and  
161 include rain gauge station data from multiple sources (regional and national meteorological services). CHIRPS  
162 data are available at a spatial resolution of 0.05° and a temporal resolution of 1-day, with a data latency period  
163 of about 3 weeks. Details of CHIRPS algorithm are available at Funk et al. (2015). Agreement between the  
164 reference (IMERG Final) and CHIRPS would indicate that the IMERG Final estimates are robust.

165

## 166 **2.4 Study Region**

167 The Niger river, with a drainage basin of 2,117,700 Km<sup>2</sup>, is the third longest river in Africa. The source of the main  
168 river is in the Guinea Highlands, and runs through Mali, Niger, on the border with Benin and then through Nigeria,  
169 discharging through a massive delta, known as the Niger Delta (the world's third largest wetland), into the Atlantic  
170 Ocean. The rainfall regimes in the region follow the seasonal migration of the Inter-Tropical Convergence Zone  
171 (ITCZ), which brings rainfall primarily in the summer season (Animashaun et al. 2020; Sorí et al. 2017).  
172 Climatologically, the Niger basin lies in three latitudinal sub-regions (Akinsanola et al. 2015, 2017): (1) the Guinea  
173 coast (latitude 4°–8°N), which borders the tropical Atlantic Ocean in the south; (2) the Savannah (latitude 8°–12°N),  
174 an intermediate sub-region; and (3) the Sahel (latitude > 12°N) to the north. The Guinea coast experiences a  
175 bimodal rainfall regime that is centered in the summer monsoon period of June–September, with August being the  
176 period of a short dry season, while the Savannah and Sahel sub-regions experience a unimodal rainfall regime, with  
177 maximum rainfall occurring in August (Akinsanola and Zhou 2018). The ranges of annual rainfall amounts are: 400–  
178 600 mm in the Sahel, 900–1200 mm in the Savannah; and 1500–2000 mm in the Guinea coast (Akinsanola et al.  
179 2017).

180

181 The Niger basin is home to eight major reservoir dams (see Table 1 and Fig. 1): (1) Selingue Dam in Mali: a primarily  
182 hydropower dam, (2) Markala Dam in Mali: a primarily irrigation dam, serving about 75,000 ha of farmland, (3)  
183 Goronyo Dam in Nigeria: a multi-purpose dam for flood control, provision of downstream water supply and the release



184 of water for irrigation in the dry season, (4) Bakolori Dam in Nigeria: a primarily irrigation dam with a command area  
 185 of about 23,000 ha, (5) Kainji Dam in Nigeria: the largest Dam on the Niger supplying power for most towns in  
 186 Nigeria, (6) Jebba Dam in Nigeria: a primarily hydropower dam, (7) Dadin Kowa Dam: a multi-purpose dam for  
 187 water supply, electricity and irrigation, (8) Lagdo Dam in Cameroon: a multi-purpose dam providing electricity to the  
 188 northern part of the country and supplying irrigation water for 15,000 hectares of cropland. The watersheds of the  
 189 dams are primarily either in the Savanna (Selingue, Markala, Jebba, Dadin Kowa, an Lagdo), or in the Sahel (Goronyo,  
 190 Kainji), or partly in both (Bakolori). The watershed sizes vary over a large range, from 4,887 Km<sup>2</sup> (Bakolori Dam) to  
 191 1,464,092 Km<sup>2</sup> (Kainji Dam). The average elevations of the watersheds are close to each other at 500 ± 50 m.a.s.l.

192  
 193 In order to make the results of this study meaningful to reservoir managers, the Niger basin was divided into  
 194 watersheds according to the locations of the dam reservoirs (see Fig. 1). Then the sub-basin of each dam was defined  
 195 as the drainage between the dam itself and the upstream dam. For example, the drainage basin of the Markala Dam  
 196 does not include the drainage basin of the Selingue Dam.

197  
 198 Table 1. Selected dams and their watershed characteristics

Dam	Country	Operational since*	Capacity (million m <sup>3</sup> )*	Power (MW)*	Primary Purpose*			Area of Drainage Basin (km <sup>2</sup> )**	Elevation of Drainage Basin (m)**
					Irrigation and Water Supply	Flood Control	Hydroelectricity		
Selingue	Mali	1982	2170	44			x	32685	473
Markala	Mali	1947	175		x			102882	442
Goronyo	Nigeria	1983	942		x	x		31547	446
Bakolori	Nigeria	1978	450		x			4887	519
Kainji	Nigeria	1968	15000	960			x	1464092	406
Jebba	Nigeria	1984	3600	540			x	40268	308
Dadin Kowa	Nigeria	1988	2855	35	x		x	32936	535
Lagdo	Cameroon	1983	7800	72		x	x	31352	452

199 \* information obtained from the Global Reservoir and Dam Database (Lehner et al. 2011) and Food and Agriculture Organization  
 200 of the United Nations (FAO)'s Global Information System on Water and Agriculture (AQUASTAT).

201 \*\* Calculated from HydroSEHDS (Lehner et al. 2008).

202  
 203  
 204 **2.5 Evaluation**

205 IMERG Final rainfall products are used in this study as reference to evaluate the performance of GFS precipitation  
 206 forecasts. The comparison period is 15 June 2019 to 15 June 2020 to match the period for which the version-15 of

207 GFS model forecasts is available. The spatial resolutions of the forecast and satellite products are different: 0.25°(GFS),  
 208 0.10° (IMERG Final and IMERG Early), and 0.05° (CHIRPS). The temporal resolutions of the satellite products are:  
 209 30-minute (IMERG Final and IMERG Early) and daily (CHIRPS). Our comparison is mostly based on sub-basin (i.e.  
 210 watershed for each dam) average values, in which case we average all the datasets to the sub-basin spatial scale. In  
 211 some cases, where we compare the spatial patterns of rainfall, we resample both IMERG products and CHIRPS to  
 212 0.25° using the bilinear interpolation technique to match the spatial resolution of GFS.

213  
 214 For evaluation metrics, we used the modified Kling-Gupta Efficiency (KGE; Gupta et al. 2009; Kling et al. 2012) and  
 215 its components: Bias Ratio (BR), correlation (R), and variability ratio ( $\gamma$ ). *KGE* measures the goodness-of-fit between  
 216 estimates of precipitation forecasts and reference observations as:

$$217 \quad KGE = 1 - \sqrt{(R - 1)^2 + (BR - 1)^2 + (\gamma - 1)^2},$$

$$218 \quad BR = \frac{\mu_f}{\mu_o},$$

$$219 \quad \gamma = \frac{CV_f}{CV_o},$$

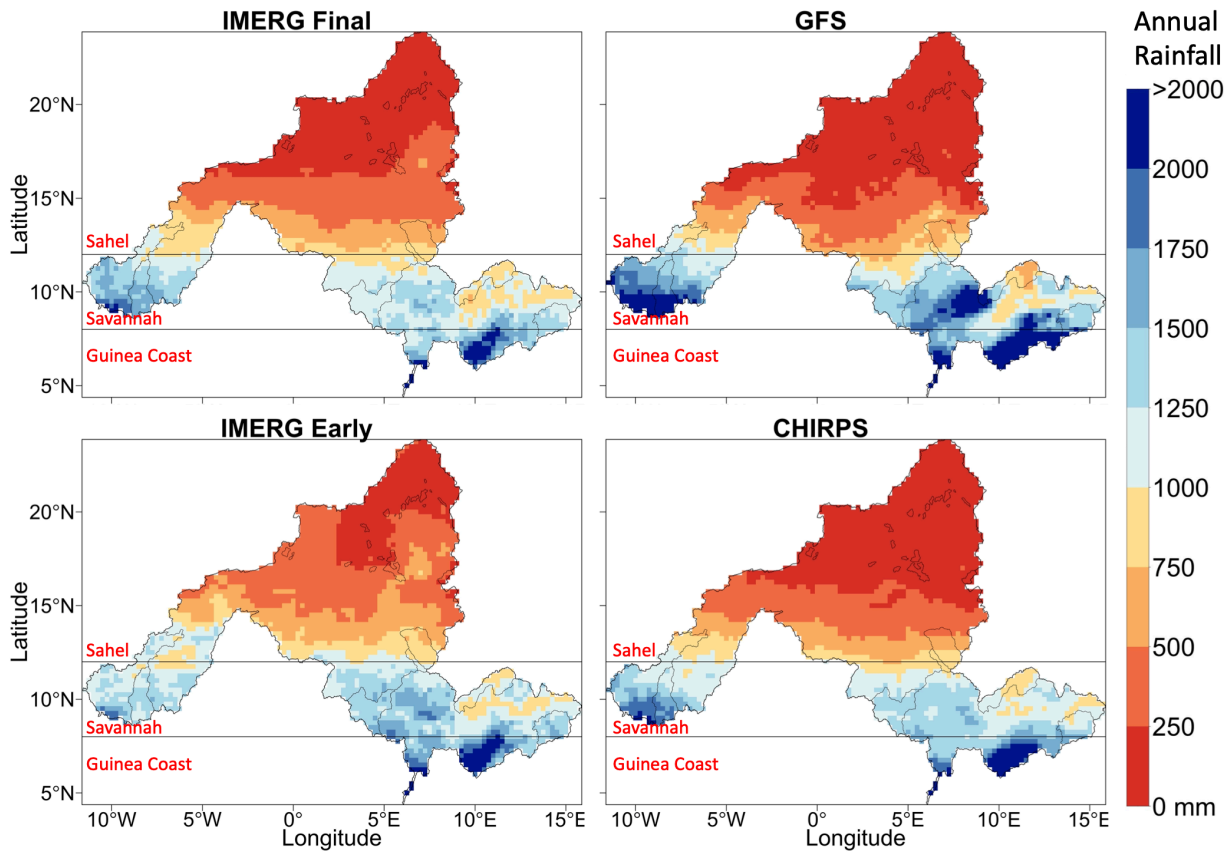
220 where R is the linear correlation coefficient between forecasted and observed precipitation, BR is the bias ratio,  $\gamma$  is  
 221 the variability ratio,  $\mu$  is the mean precipitation, CV is the coefficient of variation, and the indices *f* and *o* represent  
 222 forecasted and observed precipitation values, respectively. KGE values range from  $-\infty$  to 1, with values closer to 1  
 223 indicating better model performance. Towner et al. (2019) suggested the following classifications: “Good” ( $KGE \geq$   
 224 0.75), “Intermediate” ( $0.75 \geq KGE \geq 0.5$ ), “Poor” ( $0.5 \geq KGE > 0$ ), and “Very poor” ( $KGE \leq 0$ ). The *BR* values  
 225 greater than 1 indicate a positive bias whereby forecasts overestimate precipitation relative to the observed data,  
 226 while values less than 1 represent an underestimation. *The*  $\gamma$  values greater than 1 indicate that the variability in the  
 227 forecast time series is higher than that observed, and values less than 1 show the opposite effect. The *R* measures the  
 228 strength and direction of the linear relationship between the forecast and observed values, and to what extent the  
 229 temporal dynamics of observed rainfall is captured in the forecasts. The correlation values of 0.6 or more are  
 230 considered to be skillful (e.g., Alfieri et al. 2013). In addition, the root mean-square-error normalized by reference  
 231 precipitation mean (NRMSE) was also used.

232

233 **3. Results and Discussion**

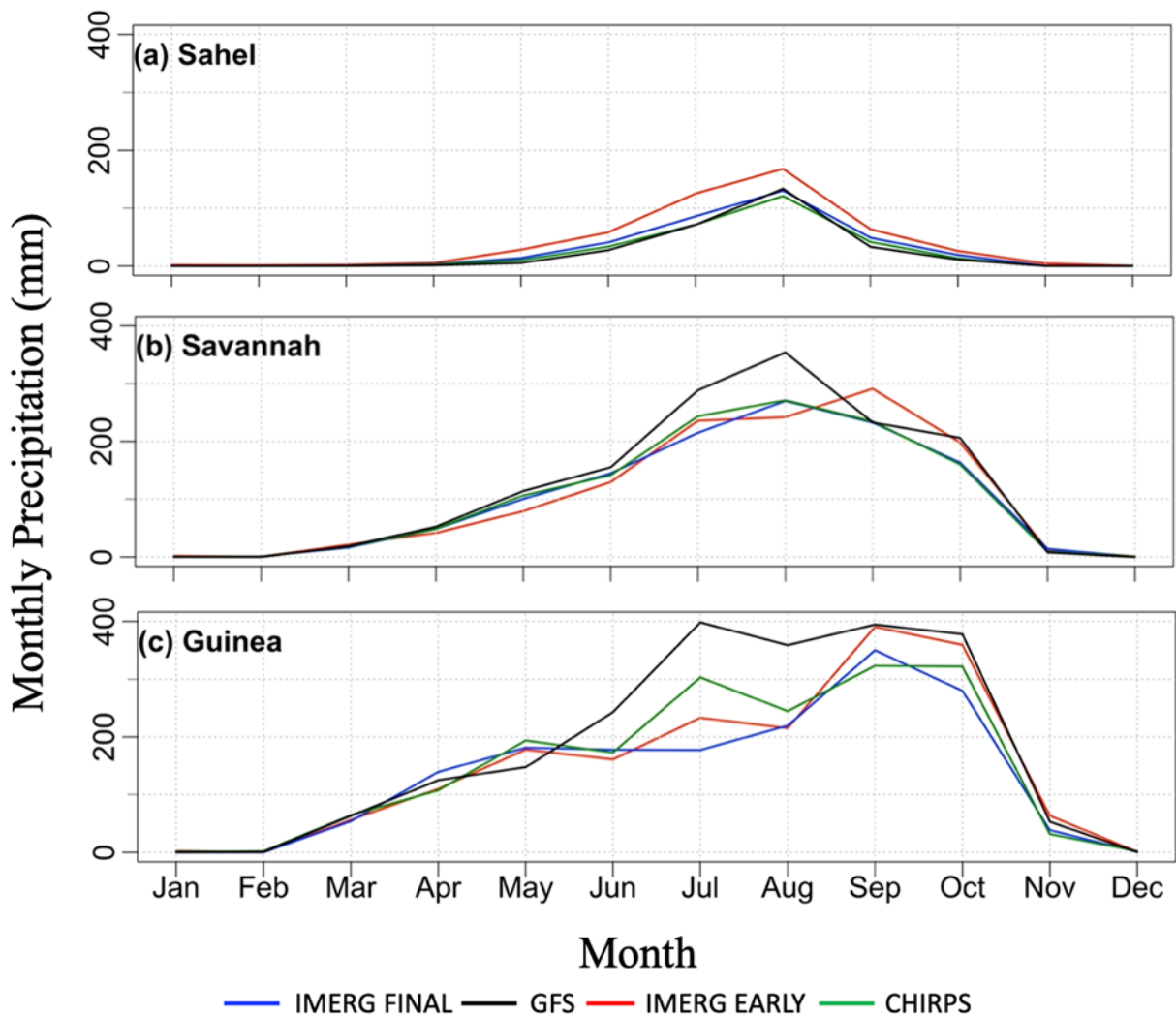
234 **3.1 Annual Spatial Variability and Seasonal Characteristics**

235 The spatial map of annual (15 June 2019 – 15 June 2020) rainfall from the various rainfall products is given in Figure  
236 2. According to the reference rainfall product (i.e. IMERG Final), the Niger basin experiences average annual rainfall  
237 of 700 mm. The spatial rainfall distribution shows north-to-south increasing gradient, with the Sahel region (> 12°N)  
238 receiving on average 346 mm per year, the Savanna region (8°N – 12°N) receiving on average 1,206 mm per year,  
239 and the Guinea region (4°N – 8°N) receiving on average 1,620 mm per year. The spatial structures (climatology and  
240 north-south gradient in rainfall) of GFS, IMERG and CHIRPS rainfall fields are quite similar to those of IMERG  
241 Final. However, the 1-day GFS tends to overestimate in the wet Guinea region of the basin, whereas both IMERG  
242 Early and CHIRPS give values that are very close to IMERG Final.



243  
244 Figure 2. Spatial map of annual rainfall (in mm), for the period 15 June 2019 to 15 June 2020, derived from (a)  
245 IMERG Final, (b) GFS (1-day lead time), (c) IMERG Early, and (d) CHIRPS.  
246

247 Figure 3 shows the seasonal rainfall pattern for each climatological region. According to the reference IMERG Final,  
 248 as one goes from north to south, the rainy season expands from 3 months (June – September) in the Sahel to 6 months  
 249 (March – November) in the Savanna and Guinea regions. The peak rainfall also shows north-south gradient, with peak  
 250 rainfall of 130 mm in the Sahel, to 269 mm in the Savanna, and 350 mm in the Guinea. The rainfall pattern is unimodal  
 251 with a peak rainfall value in August for both Sahel and Savanna, but becomes bimodal with one peak in May and the  
 252 other in September for Guinea.  
 253



254 Figure 3. Monthly precipitation regime for the three climatological zones of the Niger river Basin: (a)  
 255 Sahel, (b) Savanna, and (c) Guinea. Analyses are based on rainfall fields derived from IMERG Final, 1-  
 256 day-lead GFS, IMERG Early, and CHIRPS. The time period covers from 15 June 2019 to 15 June 2020.

257 When validated against IMERG Final, the performance of GFS in capturing the seasonal rainfall characteristics  
258 deteriorates as one goes from north to south. GFS captures both the seasonal rainfall pattern and rainfall peak in the  
259 Sahel, and captures the seasonal rainfall pattern but tends to moderately overestimate the peak in the Savannah, while  
260 it has large overestimation (almost twice as much as the reference) in the Guinea particularly during summer. As far  
261 as the other satellite products are concerned, IMERG Early tends to slightly overestimate in the Sahel across all rainy  
262 months, but performs relatively well in the Savannah and Guinea regions. CHIRPS is very close to IMERG Final in  
263 all regions and months, with the exception of modest overestimation of the July rainfall in Guinea.

264

### 265 **3.2 How well do GFS forecasts capture annual rainfall?**

266 Here, we aggregate the 1-day lead GFS forecasts to annual time scale and compare the results against corresponding  
267 annual precipitation estimates from IMERG Final. Figure 4 presents the watershed-averaged annual rainfall for each  
268 dam watershed. According to IMERG Final, the annual rainfall varies from 434 mm (in Kainji) to 1,481 mm (in  
269 Selingue). Watersheds 1 (Selingue) and 2 (Markala), located in the western part of the Savannah, receive the largest  
270 amount of rainfall, i.e., 1481 mm and 1406 mm, respectively. Watershed 3 (Markala), located in the eastern part of  
271 the Sahel, receives 741 mm of annual rainfall. Watershed 4 (Bakolori), characterized by the smallest watershed area  
272 compared to the rest of the watersheds, lies partly in the Sahel and partly in the Savannah region and receives 921 mm  
273 of annual rainfall. Watershed 5 (Kainji), characterized by the largest watershed area of all, lies mostly in the Sahel  
274 region and receives the lowest amount of annual rainfall (434 mm). Watersheds 6 (Jebba), 7 (Dadin Kowa), and 8  
275 (Lagdo), located in the Savannah, receive annual rainfall amounts of 1190 mm, 941 mm, and 1295 mm, respectively.

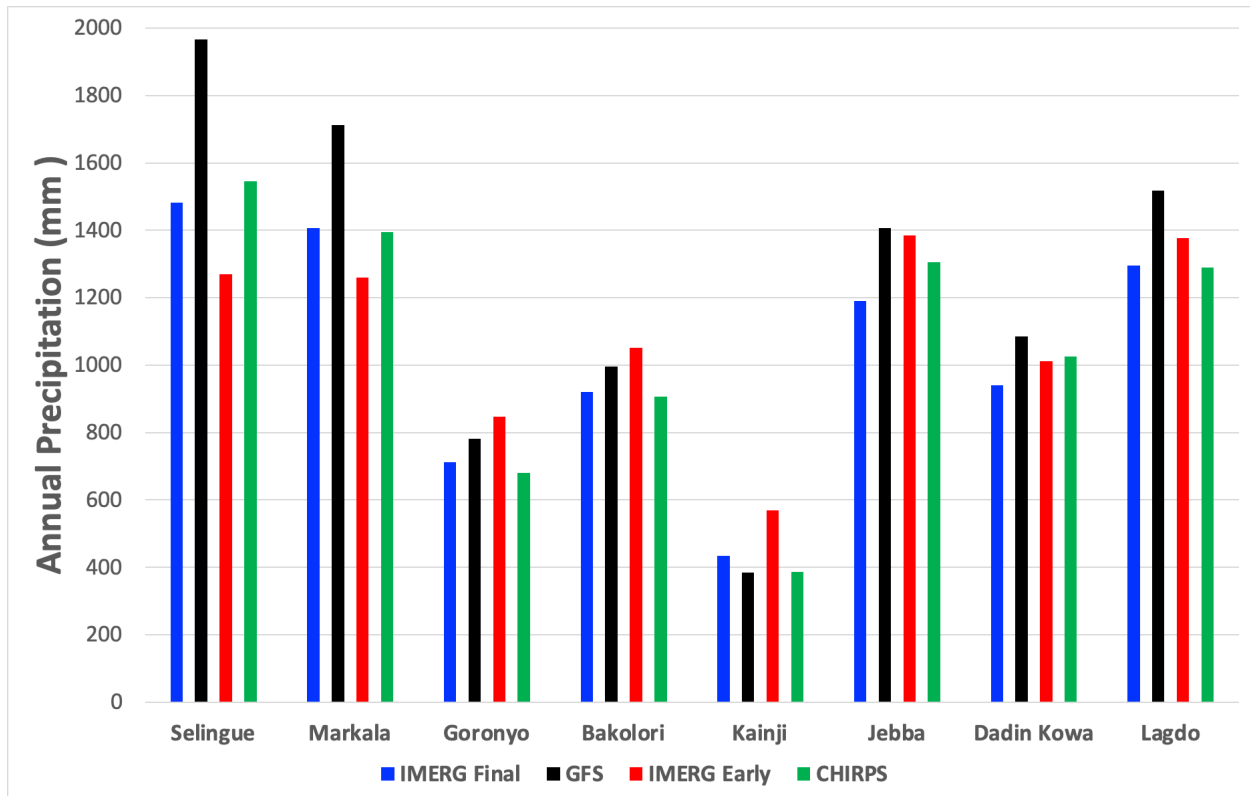
276

277 Validated against IMERG Final, the GFS tends to overestimate rainfall in all watersheds located in the Savannah (or  
278 watersheds that receive relatively large rainfall amounts), with an overestimation varying in the range 8% to 33%,  
279 with larger bias for watersheds receiving higher rainfall amount. For watersheds in the Sahel (watersheds receiving  
280 low rainfall amount), GFS gives less bias (-11% for the driest Kainji watershed and +10% for Bakolori).

281

282 In contrast, IMERG Early tends to underestimate rainfall in all watersheds located in the Savannah (with larger  
283 negative bias in watersheds with large rainfall amount) but tends to overestimate in all watersheds located in the Sahel  
284 (with very large overestimation bias for the driest watershed) Therefore, GFS and IMERG Early have different bias

285 characteristics: whereas GFS outperforms IMERG Early in the Sahelian climate where well-organized convective  
 286 systems dominate the monsoon, IMERG Early outperforms GFS in the Savannah and Guinea climate which are  
 287 characterized by short-lasting and localized systems and wet land surface conditions. CHIRPS estimates are  
 288 reasonably close to IMERG Final, indicating that the choice of reference product between CHIRPS and IMERG Final  
 289 would not substantially affect the findings on the accuracy of GFS forecasts.  
 290

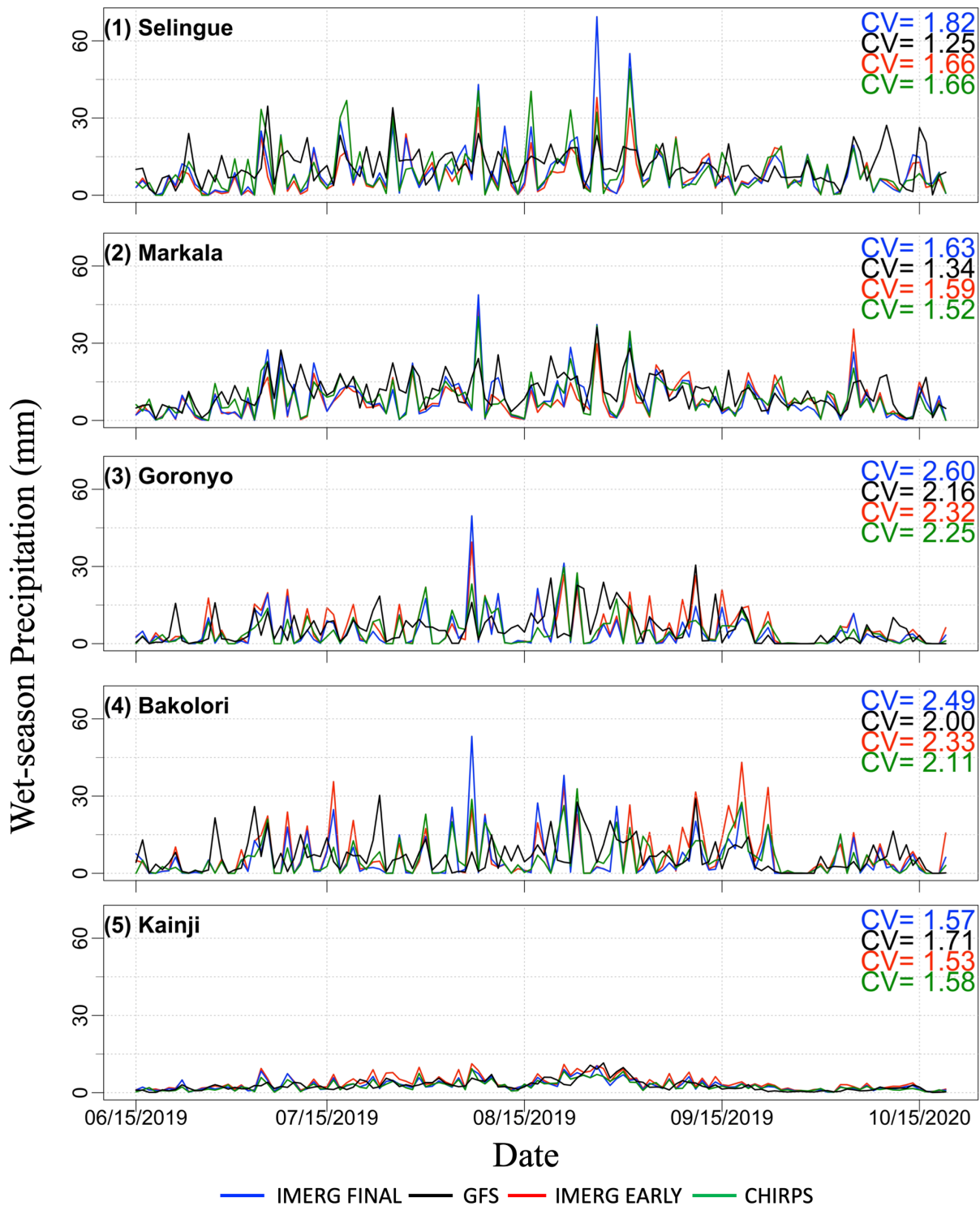


291  
 292 Figure 4. Sub-basin averaged annual precipitation (mm) for the period, 15 June 2019 to 15 June 2020, for each  
 293 of the Niger’s sub-basin, derived from the 1-day lead GFS forecast and different satellite precipitation  
 294 products.

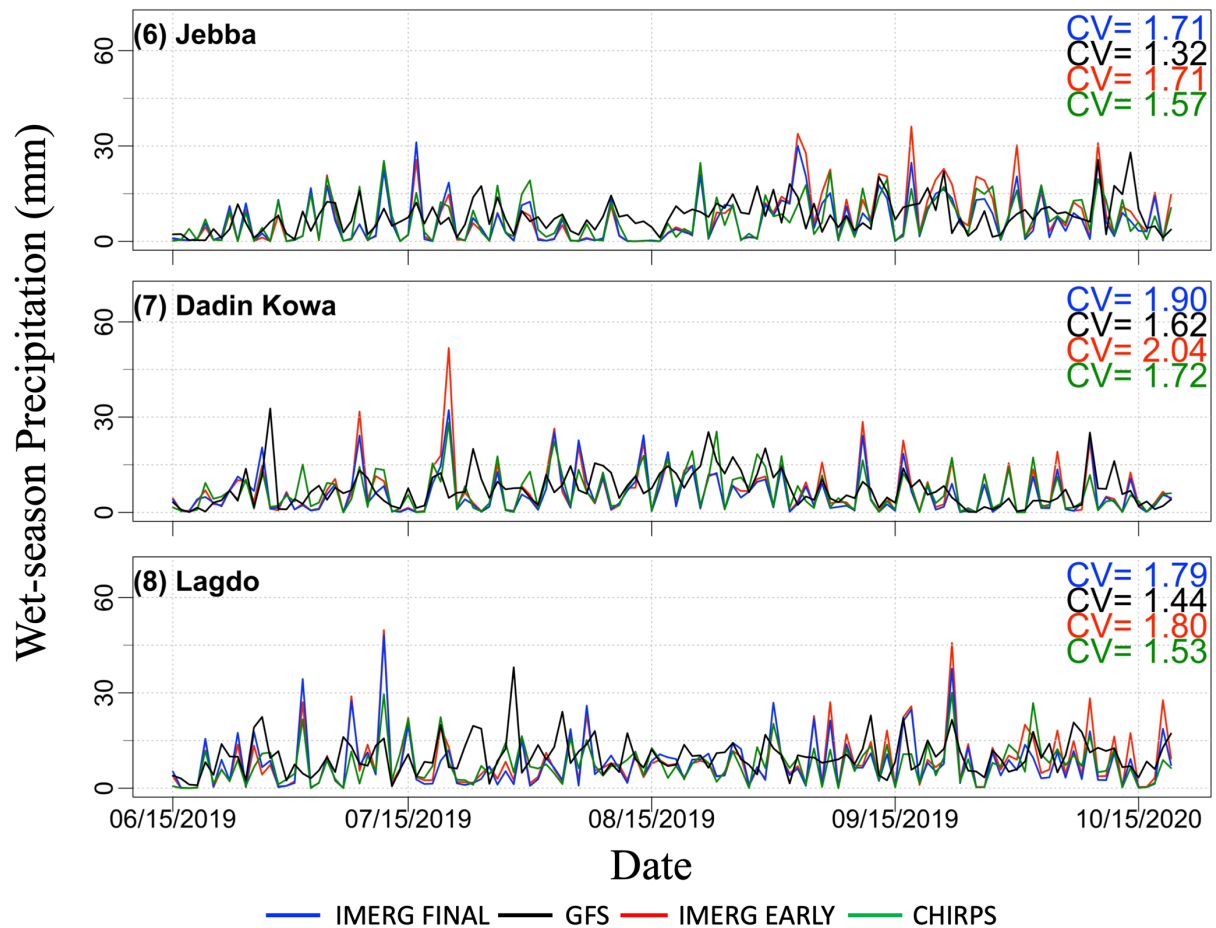
295 **3.3 How well is the time series of daily precipitation forecasted?**

296 Figures 5 and 6 present the time series of watershed-averaged daily rainfall, for the wet period June – October.  
 297 According to IMERG Final, the temporal variability (as measured through coefficient of variation or CV) varies from  
 298 1.22 to 2.60. Validated against IMERG Final, the GFS tends to underestimate the temporal variability and particularly  
 299 underestimate large spikes in rainfall, at almost all sites except at Kainji. The GFS’s relatively better performance for

300 Kainji could be attributed to the watershed's large area that results in relatively smooth temporal variability. Both  
 301 IMERG Early and CHIRPS provide CV values that are very close to IMERG Final.



302 Figure 5. Time series of sub-basin averaged precipitation total (mm) for the wet period (June – September 2019 for  
 303 all sub-basins, derived from various precipitation products, for five sub-basins. The Figure also shows the  
 304 coefficient of variation (CV) as a measure of temporal variation.



305 Figure 6. Same as in Figure 5 but for the remaining three watersheds.

306

307 Figure 7 displays the performance statistics of watershed-averaged daily rainfall (validated against IMERG Final) in  
 308 terms of Kling-Gupta Efficiency (KGE), Bias Ratio (BR), correlation (R), variability ratio ( $\gamma$ ), and root mean square  
 309 error normalized by reference precipitation mean (NRMSE). First, the performance results for the 1-day lead GFS are  
 310 considered. The KGE scores are poor ( $0.3 < KGE < 0.5$ ) for half of the watersheds considered (Selingue, Goronyo,  
 311 Bakolori, and Lagdo) and intermediate ( $0.5 < KGE < 0.75$ ) for the remaining half watersheds (Markala, Kainji, Jebba,  
 312 and Dadin Kowa). The breakdown of the KGE scores (BR, R, and  $\gamma$ ) reveals the key factors contributing to the KGE  
 313 estimates. The GFS tends to overestimate daily precipitation for most sub-basins, as BR is higher than one, except for  
 314 Kainji. The overestimation is particularly high for Selingue and Markala, where BR is 1.33 and 1.22, respectively.  
 315 The correlation coefficient between GFS and IMERG Final is mostly low ( $R < 0.60$ ), and is particularly lower for  
 316 Bakolori ( $R=0.36$ ) and Goronyo ( $R=0.43$ ). The variability ratio of GFS is mostly between 0.69 to 0.83 (except for



317 Kainji, where  $\gamma$  is 1.09), indicating that the GFS tends to give lower temporal variability of rainfall. The NRMSE is  
318 very high, ranging from 100% to 266%, and is particularly high for Goronyo (266%) and Bakolori (264%), which are  
319 relatively small-sized watersheds.

320

321 Next, the performance of IMERG Early was examined with respect to IMERG Final, mainly to assess if it is possible  
322 to use the near-real-time IMERG Early product to calibrate and improve the accuracy of GFS forecasts. The IMERG  
323 Early performs much better with KGE values higher than 0.75 (except for Kainji where KGE is 0.69), correlation  
324 higher than 0.90, and variability ratio close to the optimum value. The high performance of IMERG Early is due to its  
325 similarity with the IMERG Final product, as the main difference between the two products is that IMERG Early,  
326 unlike IMERG Final, does not use monthly rain gauge observations for bias correction. Such monthly bias correction  
327 techniques would not alter the pattern and variability of IMERG Early compared to IMERG Final. Therefore, the  
328 performance of IMERG Early should be evaluated using bias statistics, the other statistics (correlation and variability  
329 ratio) are presented for completeness. IMERG Early overestimates rainfall in most watersheds in the range 11%  
330 (Lagdo) to 28% (Kainji) except for two watersheds, where it slightly underestimates by 14% (Selingue) and 11%  
331 (Markala). Comparison of the performance of GFS and IMERG Early indicates that both products have different bias  
332 characteristics. In some watersheds (e.g., Kainji), GFS outperforms IMERG Early in terms of bias, whereas in other  
333 watersheds (e.g., Markala), IMERG Early outperforms GFS.

334

335 CHIRPS was also compared with IMERG Final to assess how the use of different reference products may affect the  
336 finding about the performance of GFS forecasts. The KGE scores of CHIRPS are higher than 0.75 in all cases,  
337 indicating that CHIRPS and IMERG Final have comparable KGE performance. Therefore, the performance of GFS  
338 is expected to be about the same even if the reference product used this in this study (IMERG Final) changes to  
339 CHIRPS.

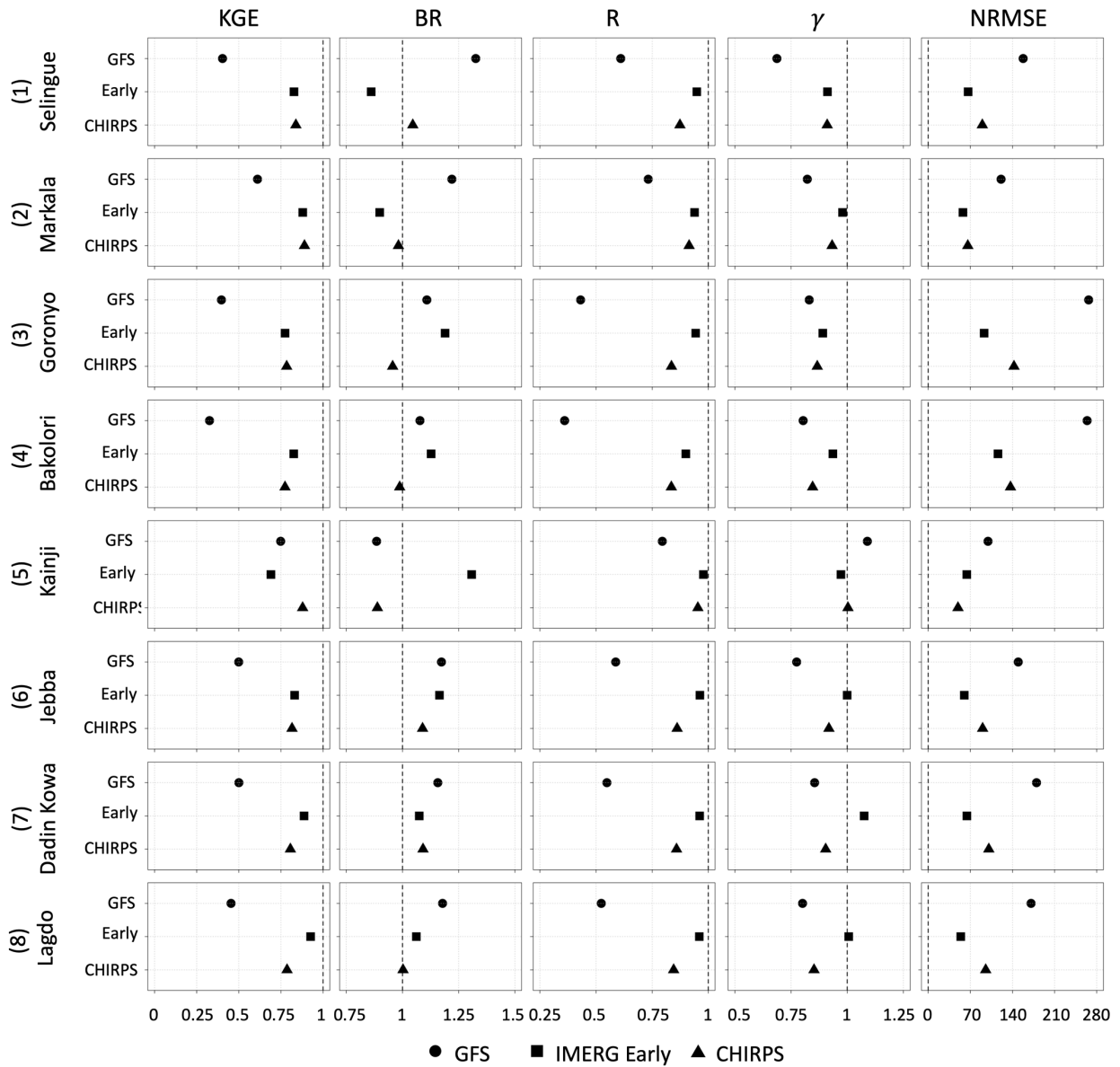
340

341

342

343

344

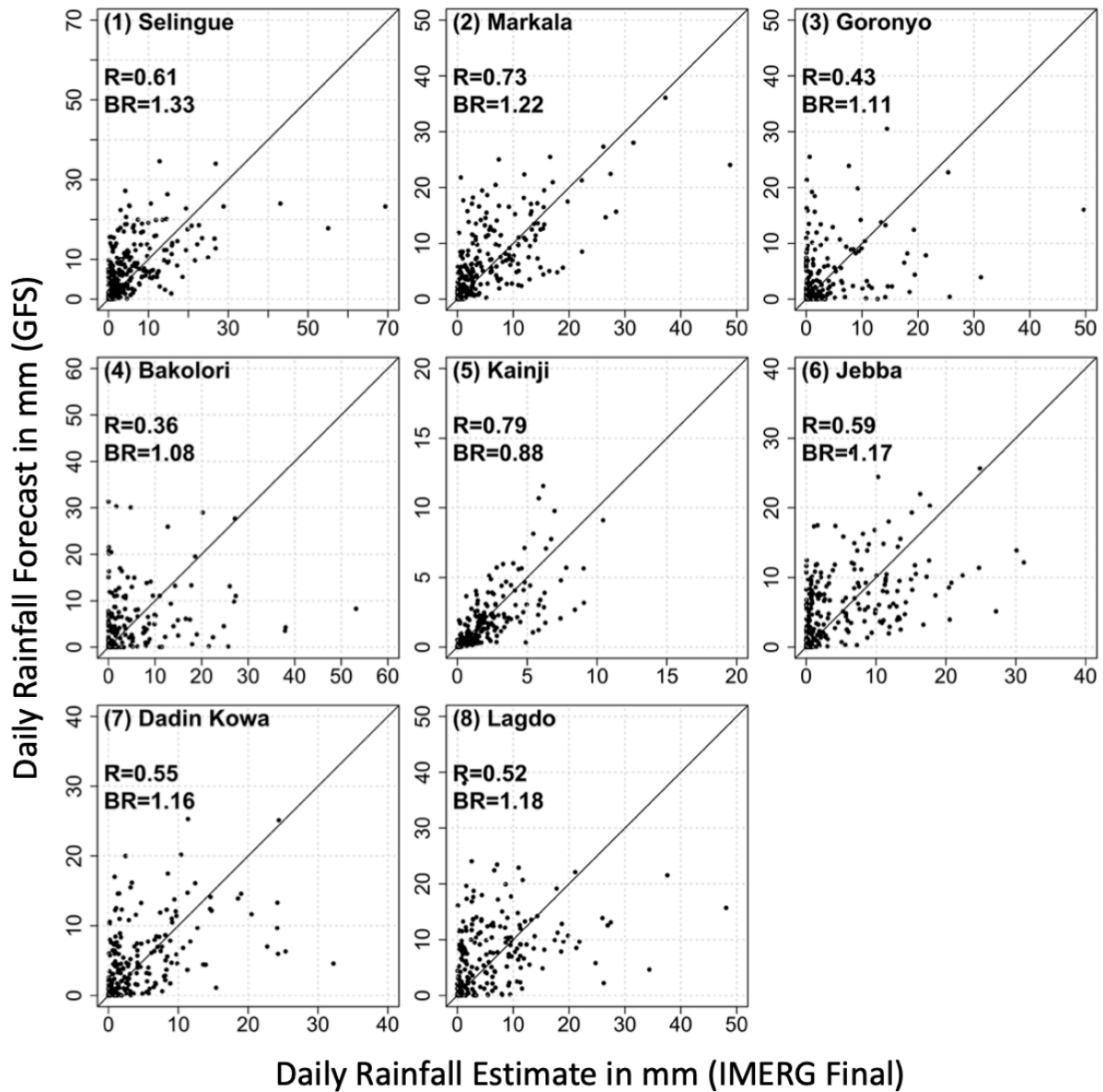


346

347 Figure 7. Summary of performance statistics (Kling-Gupta Efficiency KGE, Bias Ratio BR, correlation R,  
 348 variability ratio  $\gamma$ , and root mean square error normalized by reference rainfall [%], for the 1-day lead time GFS  
 349 forecasts and other satellite products. The time period considered was June 15, 2019 – June 15, 2020.  
 350

351 **3.4 Dependence of Forecast Performance on Precipitation Rate**

352 Figure 8 presents the scatterplot of 1-day lead GFS forecasts and IMERG Final at daily and watershed-average scales.  
 353 The performance of GFS varies between watersheds. In the Markala and Kainji watersheds, GFS forecasts agree well  
 354 with IMERG Final at almost all rain rates. In the Selingue watershed, GFS agrees well with IMERG Final for rain  
 355 rates under 30 mm/day, but GFS substantially underestimates all rain rates above 30 mm/day. In the remaining five  
 356 watersheds, GFS has poor performance, replete with large scatter, high false alarm, and large underestimation bias of  
 357 heavy rain rates.



358 Figure 8. Scatterplot of watershed-averaged daily precipitation forecast obtained from 1-day lead GFS  
 359 forecasts against corresponding values from IMERG Final.

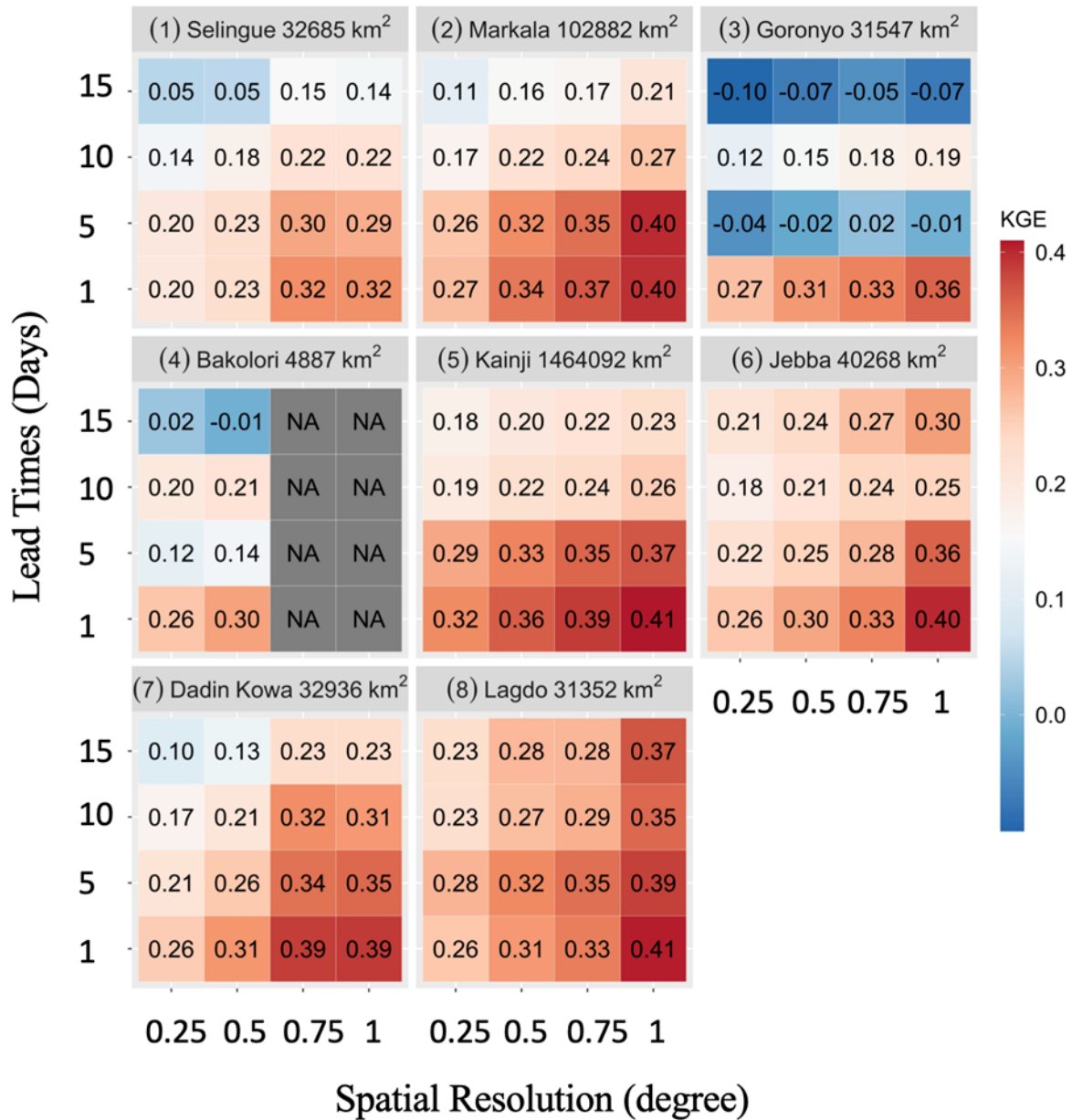
### 360 **3.5 Dependence of Daily Forecast Performance on Lead Time and Spatial Scale**

361 In order to assess the effect of various lead times and spatial scales on forecast performance, we obtained daily GFS  
362 forecasts at various lead times (1-day, 5-day, 10-day, and 15-day), and aggregated the forecasts at spatial scales from  
363  $0.25^\circ$  to coarser scales ( $0.5^\circ$ ,  $0.75^\circ$ , and  $1^\circ$ ) by averaging grids. The purpose of degrading the resolution is to determine  
364 at which resolution the forecasts have acceptable performance. The KGE value at each spatial resolution was  
365 calculated in the following steps: (i) average the data at the required spatial resolution, (ii) extract pairs of data (one  
366 from IMERG Final, and the other from GFS), (iii) concatenate the pairs to form one large series of data, and (4)  
367 compute a single KGE from this data series. The resulting KGE values are shown in Fig. 9.

368  
369 With regard to the effect of spatial scales, the KGE at the GFS native resolution (i.e.  $0.25^\circ$ ) is very low. As the spatial  
370 scale increases, KGE increases, as expected. For instance, for Markala watershed KGE increases from 0.27 ( $0.25^\circ$ ) to  
371 0.40 ( $1^\circ$ ) for a 1-day lead. This indicates that the variation in KGE values between the watersheds could be partly  
372 explained by the watershed size. For example, based on Fig. 5, the KGE for the 1-day lead daily GFS forecast was the  
373 highest for the largest Kainji watershed (watershed area of 1,464,092  $\text{Km}^2$ ) and the lowest for the smallest Bakolori  
374 watershed (4,887  $\text{Km}^2$ ). With regard to the effect of lead time for daily forecasts, KGE decreases significantly as lead  
375 time increases. For instance, for Markala watershed and a grid size of  $1^\circ$ , KGE decreases from 0.40 (1-day lead) to  
376 0.21 (15-day lead).

377

378

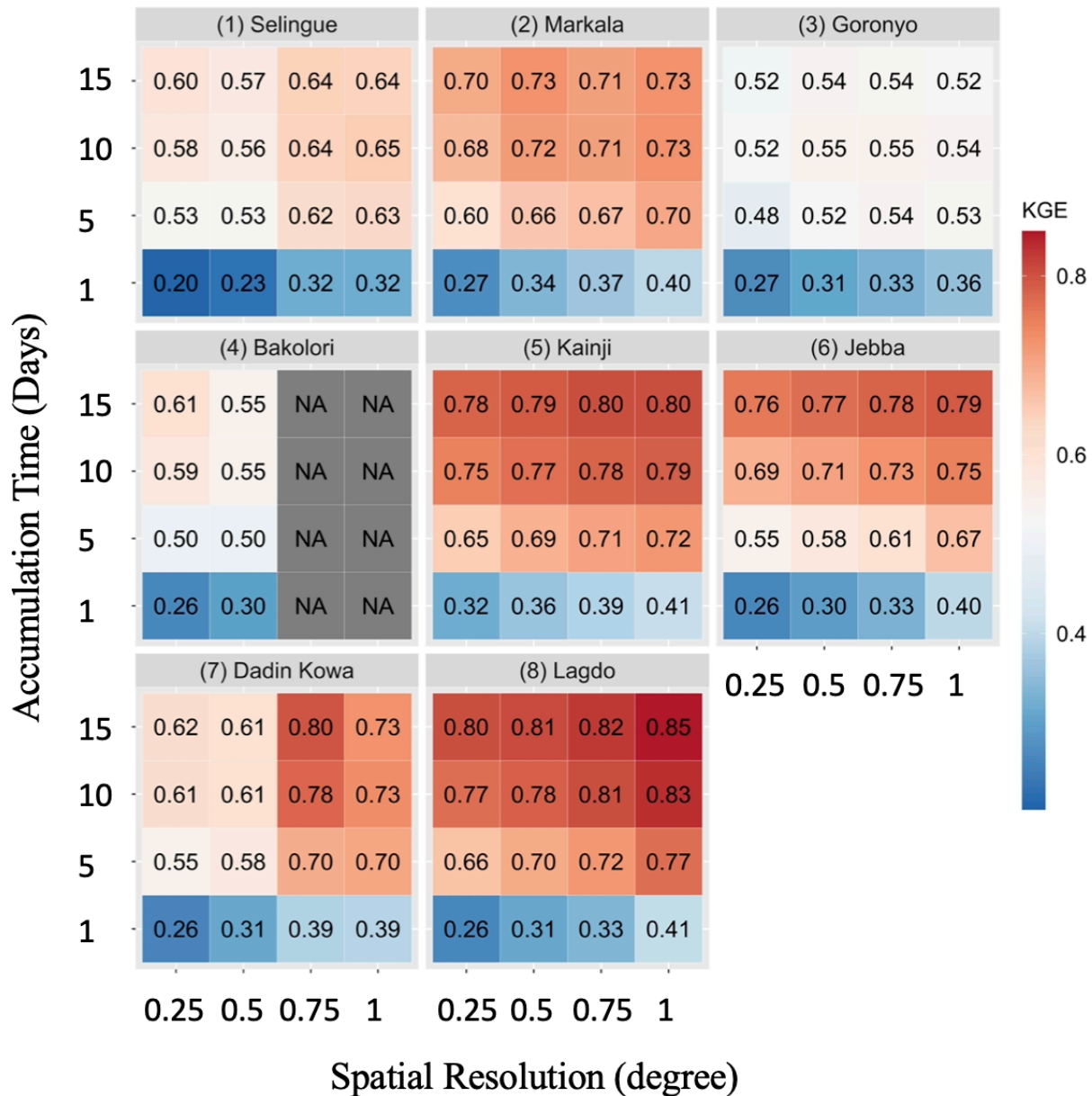


380  
 381 Figure 9. Kling-Gupta Efficiency (KGE) for daily precipitation of GFS as a function of lead time (1-day, 5-day, 10-  
 382 day, and 15-day) and spatial scale (0.25°, 0.50°, 0.75°, 1.0°). The dam names and corresponding watershed areas are  
 383 given in the titles.  
 384

385 **3.6 Effect of Temporal Aggregation Scale on Forecast Performance**

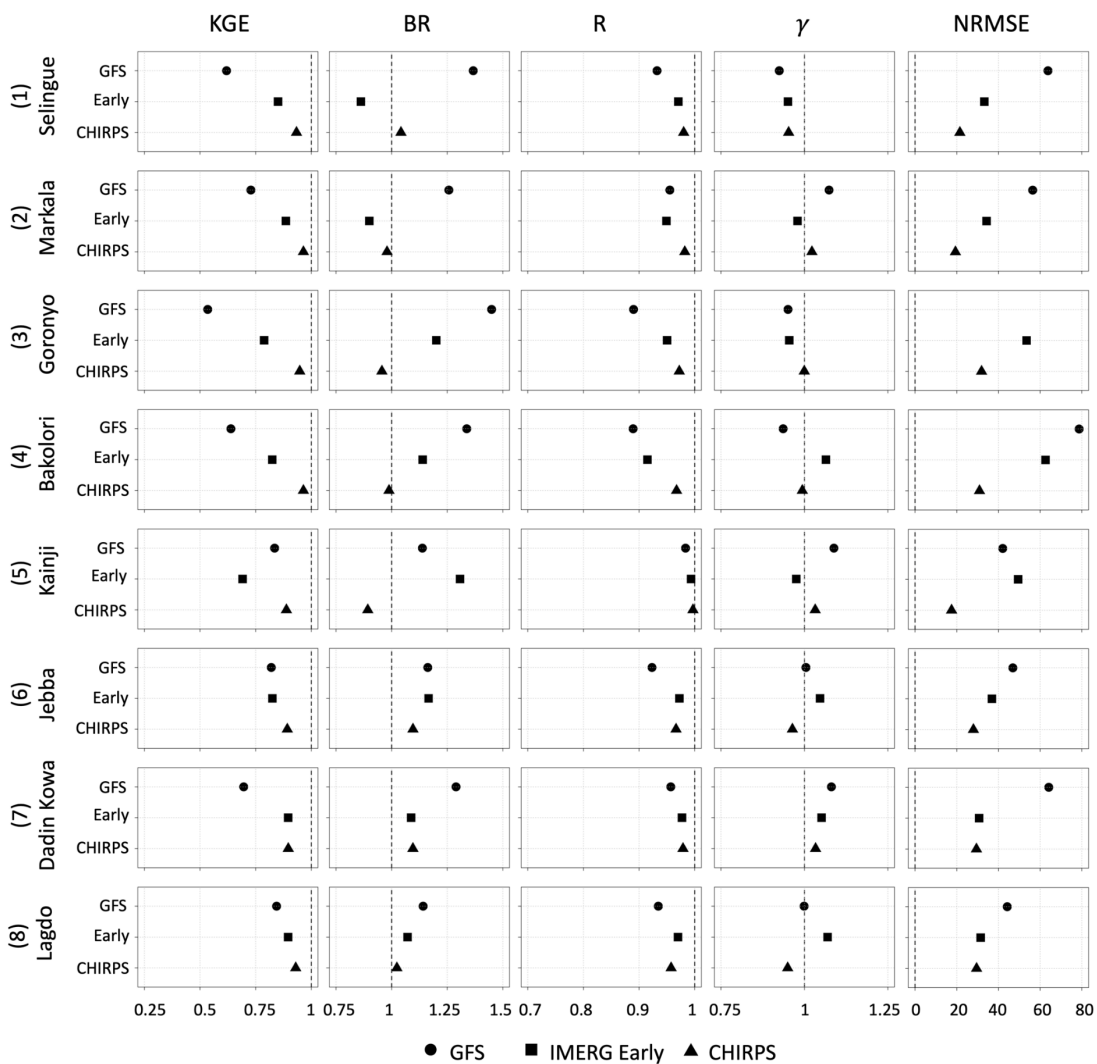
386 To assess the effect of temporal aggregation scale, we obtained the 1-day total, 5-day total, 10-day total, and 15-day  
 387 total GFS precipitation forecasts. These multi-day forecasts are constructed by combining multiple lead-time forecasts.  
 388 For instance, the 5-day total forecast is obtained by adding the 1-day lead, 2-day lead, 3-day lead, 4-day lead, and 5-

389 day lead daily forecasts. Figure 10 presents the KGE values for GFS forecasts over different temporal aggregation  
 390 scales, and different grid sizes. Temporal aggregation substantially increases KGE at all spatial scales. For example,  
 391 at the grid size of 1° over Markala watershed, the KGE values jump from 0.40 at daily timescale to 0.73 at 15-day  
 392 total timescale.

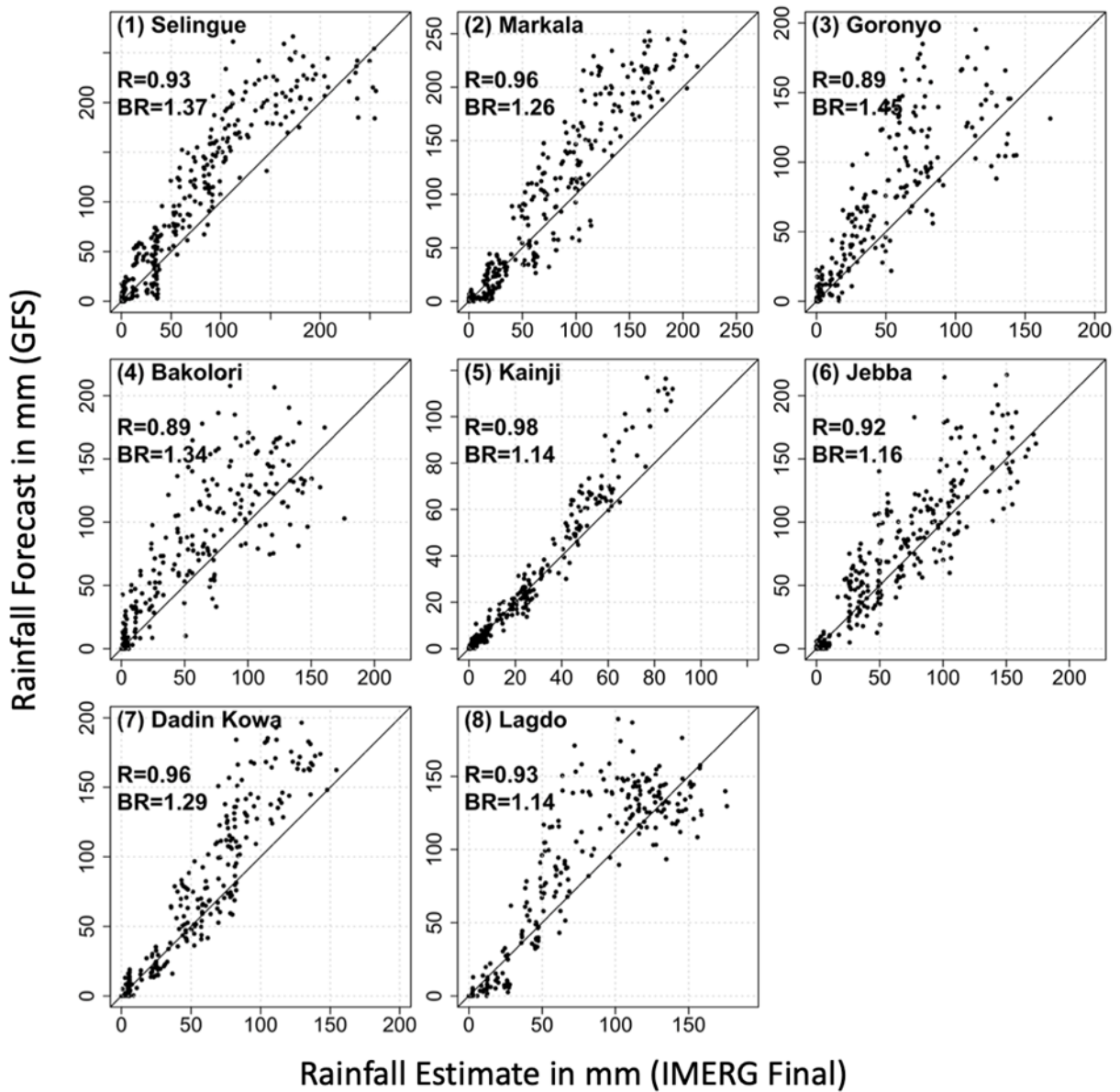


393 Figure 10. Kling-Gupta Efficiency (KGE) of GFS as a function of accumulation time scale (1-day, 5-day, 10-day,  
 394 and 15-day) and spatial scale (0.25°, 0.50°, 0.75°, 1.0°).  
 395

396 In Figure 11, we show the performance statistics of GFS for 15-day accumulated watershed-averaged rainfall forecast.  
 397 The KGE values are intermediate ( $0.5 < KGE < 0.75$ ) for four watersheds and good ( $KGE > 0.75$ ) for the remaining  
 398 four watersheds. Analysis of the components of KGE reveals that the improvement of KGE at longer timescales comes  
 399 as a result of improved correlation and variability ratio. At the 15-day accumulation timescale, IMERG Early estimates  
 400 have less bias than GFS at all watersheds, except at Kainji watershed. Figure 12 presents the scatterplot of 15-day  
 401 accumulated GFS forecast vs IMERG Final. In general, the GFS estimates perform well for low to moderate rain rates,  
 402 but tend to overestimate higher rain rates. This is consistent with Wang et al. (2019) who reported the difficulty of  
 403 capturing the magnitude of high rain rates in GFS model.



404 Figure 11. Summary of performance statistics (Kling-Gupta Efficiency KGE, Bias Ratio BR, correlation R,  
 405 variability ratio  $\gamma$ , and root mean square error normalized by reference rainfall [%], for the 15-day accumulated GFS  
 406 forecast and other satellite products.  
 407



408  
 409 Figure 12. Scatterplot of watershed-averaged 15-day accumulated precipitation forecast obtained from GFS forecast  
 410 against corresponding values from IMERG Final.  
 411

412 **4. Conclusions**

413 This study has evaluated the accuracy of medium-range (1-day to 15-day lead time) forecasts available from the Global  
 414 Forecast System (GFS), for the watersheds of large dams in the Niger river basin. Despite the limited temporal  
 415 coverage, some consistent features emerged from this evaluation. The accuracy of GFS forecast depends on climatic  
 416 regime, lead time, accumulation timescale, and spatial scale. With regard to the role of climatic regimes, the GFS



417 forecast has large overestimation bias in the Guinea (wet climatic regime), moderate overestimation bias in the  
418 Savannah (moderately wet climatic regime), but has no bias in the Sahel (dry climate). With regard to lead time, as  
419 the lead time increases, the forecast accuracy decreases. Averaging the forecasts at coarser spatial scales leads to  
420 increased forecast accuracy. For daily rainfall forecasts, the performance of GFS is very low ( $KGE < 0.32$ ) at almost  
421 all watersheds except at Markala ( $KGE = 0.44$ ) and Kainji ( $KGE = 0.68$ ), both of which have much larger watershed  
422 areas compared to the other watersheds. Averaging the forecasts at longer time scales also leads to increased forecast  
423 accuracy. For 15-day rainfall accumulation timescale, the KGE values are either “intermediate” (i.e.,  $0.50 \leq KGE \leq$   
424  $0.75$ ) for half of the watersheds (Selingue, Goronyo, Bakolori, and Daddin Kowa) or “good” (i.e.,  $KGE \geq 0.75$ ) for  
425 the remaining half (Markaa, Kainji, Jebba, and Lagdo). With regard to the effect of rainfall rate, the 15-day  
426 accumulated GFS forecasts tend to perform better for low to medium rain rates, but contain large overestimation bias  
427 at high rain rates.

428  
429 The performance statistics of GFS indicate the need for calibrating GFS forecasts in order to improve their accuracy.  
430 Post-processing calibration of GFS forecasts requires the use of “relatively better performing” and “available in near-  
431 real-time” independent rainfall observations to correct real-time dynamical GFS model forecasts. This study has  
432 compared the performance of IMERG Early satellite rainfall products with the performance of GFS in terms of bias.  
433 In the Guinea and Savannah regions, IMERG Early outperforms GFS in terms of bias, while in the dry Sahel region,  
434 IMERG Early is outperformed by GFS.

435  
436 We acknowledge that the reference dataset used in our evaluation (i.e., IMERG Final) has its own estimation errors.  
437 We conducted additional assessment to evaluate the performance of IMERG Final with respect to another independent  
438 and high-quality (i.e. satellite-gauge merged) rainfall product (i.e. CHIRPS). Our results show that IMERG Final and  
439 CHIRPS have similar rainfall characteristics, indicating the robustness of IMERG Final.

440  
441 Overall, we conclude that the GFS forecasts, at 15-day accumulation timescale, have acceptable performance,  
442 although they tend to overestimate high rain rates. The shorter the time scale, the lower is the GFS performance. We  
443 recommend identifying suitable post-processing calibration techniques, through the use of near-real time products,  
444 such as, IMERG Early, that could improve the performance of GFS, particularly in the wet Guinea and Savannah

445 regions. Possible calibration methods that could be explored include: simple bias (multiplicative) correction, multi-  
446 resolution bias correction through wavelet analysis wavelet analysis or empirical mode decomposition method, and  
447 Artificial-based methods such as Feed Forward Neural Network (FFNN), Support Vector Machine (SVR), and  
448 Adaptive Neural Fuzzy Inference System (ANFIS).

449

450

451

452

453

454

455

456

457

458

459

460

461

462

463

464

465

466

467

468

469

470

471

472

473 **5. Data and Code Availability**

474 We acknowledge the National Center for Atmospheric Research (NCAR) for providing public access to the GFS  
475 rainfall forecast data products (<https://rda.ucar.edu/datasets/ds084.1/>), NASA for providing public access to IMERG  
476 Final and IMERG Early rainfall data products (<https://disc.gsfc.nasa.gov>), and the University of California Santa  
477 Barbara's (UCSB) Climate Hazard's group for providing public access to CHIRPS rainfall data  
478 (<https://www.chc.ucsb.edu/data>).

479

480

481 **6. Author Contribution**

482 H. Yue: data processing, data analysis, and manuscript preparation; M. Gebremichael: project oversight, method  
483 design, contribution to manuscript text; V. Nourani: method design, contribution to manuscript text.

484

485

486 **7. Competing Interests**

487 The authors declare that they have no conflict of interest.

488

489

490 **8. Acknowledgement**

491 We acknowledge funding support from NASA Precipitation Measurement Mission through Grant # 80NSSC19K0688.

492

493 **References**

- 494 Abdalla, S., Janssen, P. A., Balmaseda, M. A., Mogensen, K., Bidlot, J. R., & Keeley, S.: ECMWF Experience In  
 495 Global Monitoring And Validation Of Radar Altimetry Products. In ESA Living Planet Symposium 2013, 9-13 Sep.  
 496 2013, Edinburgh, ESA Proceedings No. SP-722 (CD), 2013 December
- 497 Akinsanola, A. A., and Zhou, W.: Projections of West African summer monsoon rainfall extremes from two CORDEX  
 498 models. *Climate Dynamics*, 52(3), 2017-2028, doi:10.1007/s00382-018-4238-8, 2018
- 499 Akinsanola, A. A., Ogunjobi, K. O., Gbode, I. E., and Ajayi, V. O.: Assessing the capabilities of three regional climate  
 500 models over CORDEX Africa in simulating West African summer monsoon precipitation. *Advances in Meteorology*,  
 501 doi:10.1155/2015/935431, 2015.
- 502 Akinsanola, A.A., Ajayi, V.O., Adejare, A.T., Adeyeri, O.E., Gbode, I.E., Ogunjobi, K.O., Nikulin, G. and Abolude,  
 503 A.T.: Evaluation of rainfall simulations over West Africa in dynamically downscaled CMIP5 global circulation  
 504 models. *Theoretical and applied climatology.*, 132(1), 437-450, doi:10.1007/s00704-017-2087-8, 2017.
- 505 Alexander, S., Yang, G., Addisu, G., and Block, P.: Forecast-informed reservoir operations to guide hydropower and  
 506 agriculture allocations in the Blue Nile basin, Ethiopia. *International Journal of Water Resources Development*, 1-26,  
 507 doi:10.1080/07900627.2020.1745159, 2020
- 508 Alfieri, L., Burek, P., Dutra, E., Krzeminski, B., Muraro, D., Thielen, J., and Pappenberger, F.: GloFAS—global  
 509 ensemble streamflow forecasting and flood early warning. *Hydrology and Earth System Sciences*, 17(3), 1161-1175,  
 510 doi:10.5194/hess-17-1161-2013, 2013
- 511 Animashaun, I. M., Oguntunde, P. G., Akinwumiju, A. S., and Olubanjo, O. O.: Rainfall Analysis over the Niger  
 512 Central Hydrological Area, Nigeria: Variability, Trend, and Change point detection. *Scientific African*, 8, e00419,  
 513 doi: 10.1016/j.sciaf.2020.e00419, 2020
- 514 Arakawa, A., and Schubert, W. H.: Interaction of a cumulus cloud ensemble with the large-scale environment, Part I.  
 515 *Journal of the Atmospheric Sciences*, 31(3), 674-701, 1974.
- 516 Bhuiyan, M.A., Nikolopoulos. E.I., and Anagnostou, E.N.: Machine Learning-Based Blending of Satellite and  
 517 Reanalysis Precipitation Datasets: A Multiregional Tropical Complex Terrain Evaluation, *Journal of*  
 518 *Hydrometeorology*, 20(11), 2147-2161, doi: 10.1175/JHM-D-19-0073.1, 2019.
- 519 Bliedernicht, J., Waongo, M., Salack, S., Seidel, J., Laux, P., and Kunstmann, H.: Quality and value of seasonal  
 520 precipitation forecasts issued by the West African regional climate outlook forum. *Journal of Applied Meteorology*  
 521 *and Climatology*, 58(3), 621-642, doi:10.1175/JAMC-D-18-0066.1, 2019.
- 522 Breuer, N. E., Fraise, C.W., and Cabrera, V.E.: The Cooperative Extension Service as a boundary organization for  
 523 diffusion of climate forecasts: A 5-year study. *Journal of Extension*, 48(4), 2010, Article Number 4RIB7, 5 pp.
- 524 Chen, F., Janjić, Z., and Mitchell, K. Impact of atmospheric surface-layer parameterizations in the new land-surface  
 525 scheme of the NCEP mesoscale Eta model. *Boundary-Layer Meteorology*, 85(3), 391-421, doi:  
 526 10.1023/A:1000531001463, 1997.
- 527 Clough, S., Shephard, M., Mlawer, E., Delamere, J., Iacono, M., Cady-Pereira, K., Boukabara, S., and Brown, P.:  
 528 Atmospheric radiative transfer MODELING: A summary of the AER codes. *Journal of Quantitative Spectroscopy*  
 529 *and Radiative Transfer*, 91(2), 233-244. doi:10.1016/j.jqsrt.2004.05.058, 2005.
- 530 Dembélé, M., Schaefli, B., van de Giesen, N., and Mariéthoz, G.: Suitability of 17 rainfall and temperature gridded  
 531 datasets for largescale hydrological modelling in West Africa. *Hydrol. Earth Syst. Sci. Discuss.*, <https://doi.org/10.5194/hess-2020-68>, in review, 2020
- 533 Dezfuli, A. K., Ichoku, C. M., Huffman, G. J., Mohr, K. I., Selker, J. S., Van De Giesen, N., Hochreutener, R., and  
 534 Annor, F. O.: Validation of IMERG precipitation in Africa. *Journal of hydrometeorology*, 18(10), 2817-2825, doi:  
 535 10.1175/JHM-D-17-0139.1, 2017a
- 536 Dezfuli, A. K., Ichoku, C. M., Mohr, K. I., & Huffman, G. J.: Precipitation characteristics in West and East Africa  
 537 from satellite and in situ observations. *Journal of Hydrometeorology*, 18(6), 1799-1805, doi:10.1175/JHM-D-17-  
 538 0068.1, 2017b

539 Funk, C., Peterson, P., Landsfeld, M., Pedreros, D., Verdin, J., Shukla, S., Husak, G., Rowland, J., Harrison, L., Hoell,  
540 A., and Michaelsen, J.: The climate hazards infrared precipitation with stations—a new environmental record for  
541 monitoring extremes. *Scientific data*, 2(1), 1-21, doi:10.1038/sdata.2015.66, 2015.

542 Gossett, M., Alcoba, M., Roca, R., Cloche, S., and Urbani, G.: Evaluation of TAPEER daily estimates and other GPM-  
543 era products against dense gauge networks in West Africa, analysing ground reference uncertainty. 144(1), 255-269,  
544 doi: 10.1002/qj.3335, 2018.

545 Grell, G. A.: Prognostic evaluation of assumptions used by cumulus parameterizations. *Monthly weather review*,  
546 121(3), 764-787, doi: 10.1175/1520-0493(1993)121<0764:PEOAUB>2.0.CO;2, 1993.

547 Gupta, H. V., Kling, H., Yilmaz, K. K., and Martinez, G. F.: Decomposition of the mean squared error and NSE  
548 performance criteria: Implications for improving hydrological modelling. *Journal of hydrology*, 377(1-2), 80-91, doi:  
549 10.1016/j.jhydrol.2009.08.003, 2009.

550 Haile, A. T., Tefera, F. T., and Rientjes, T.: Flood forecasting in Niger-Benue basin using satellite and quantitative  
551 precipitation forecast data. *International journal of applied earth observation and geoinformation*, 52, 475-484, doi:  
552 10.1016/j.jag.2016.06.021, 2016.

553 Hou, A. Y., Kakar, R. K., Neeck, S., Azarbarzin, A. A., Kummerow, C. D., Kojima, M., Oki, R., Nakamura, K., and  
554 Iguchi, T.: The global precipitation measurement mission. *Bulletin of the American Meteorological Society*, 95(5),  
555 701-722, doi:10.1175/BAMS-D-13-00164.1, 2014.

556 Huffman, G. J., Adler, R., Bolvin, D., and E. Nelkin, E.: The TRMM Multi-Satellite Precipitation Analysis (TMPA).  
557 *Satellite Rainfall Applications for Surface Hydrology*, M. Gebremichael and F. Hossain, Eds., Springer, 3–22, 2010.

558 Huffman, G. J., Bolvin, D. T., Braithwaite, D., Hsu, K., Joyce, R., Xie, P., & Yoo, S. H.: NASA global precipitation  
559 measurement (GPM) integrated multi-satellite retrievals for GPM (IMERG). *Algorithm Theoretical Basis Document*  
560 (ATBD) Version, 4, 26, 2015.

561 Huffman, G. J., Bolvin, D. T., Nelkin, E. J., Wolff, D. B., Adler, R. F., Gu, G., Hong, Y., Bowman, K.P. and Stocker,  
562 E. F.: The TRMM Multisatellite Precipitation Analysis (TMPA): Quasi-Global, Multiyear, Combined-Sensor  
563 Precipitation estimates at fine scales. *Journal of Hydrometeorology*, 8(1), 38-55. doi:10.1175/jhm560.1, 2007.

564 Huffman, G.J., Stocker, E.F., Bolvin, D.T., Nelkin, E.J., Jackson J.: GPM IMERG Final Precipitation L3 1 day 0.1  
565 degree x 0.1 degree V06, Edited by Andrey Savtchenko, Greenbelt, MD, Goddard Earth Sciences Data and  
566 Information Services Center (GES DISC), Accessed: [Feb 11, 2021], doi:10.5067/GPM/IMERGDF/DAY/06, 2019a

567 Huffman, G.J., Stocker, E.F., Bolvin, D.T., Nelkin, E.J., Jackson J.: GPM IMERG Early Precipitation L3 1 day 0.1  
568 degree x 0.1 degree V06, Edited by Andrey Savtchenko, Greenbelt, MD, Goddard Earth Sciences Data and  
569 Information Services Center (GES DISC), Accessed: [Feb 11, 2021], doi:10.5067/GPM/IMERGDE/DAY/06, 2019b

570 Iacono, M. J., Mlawer, E. J., Clough, S. A., and Morcrette, J. J.: Impact of an improved longwave radiation model,  
571 RRTM, on the energy budget and thermodynamic properties of the NCAR community climate model, CCM3. *Journal*  
572 *of Geophysical Research: Atmospheres*, 105(D11), 14873-14890, doi: 10.1029/2000JD900091, 2000.

573 Jiang, M., Feng, J., Li, Z., Sun, R., Hou, Y. T., Zhu, Y., Wan, B., Guo, J., and Cribb, M.: Potential influences of  
574 neglecting aerosol effects on the NCEP GFS precipitation forecast. *Atmospheric Chemistry and Physics*, 17(22),  
575 13967–13982, doi: 10.5194/acp-17-13967-2017, 2017.

576 JMA.: Outline of the operational numerical weather prediction at the Japan Meteorological Agency (Appendix to  
577 WMO numerical weather prediction progress report). Japan Meteorological Agency, 47pp. (available online  
578 at <https://www.jma.go.jp/jma/jma-eng/jma-center/nwp/outline2019-nwp/index.htm>; last accessed: February 2021),  
579 2019.

580 Kling, H., Fuchs, M., and Paulin, M.: Runoff conditions in the upper Danube basin under an ensemble of climate  
581 change scenarios. *Journal of Hydrology*, 424, 264-277, 2012.

582 Koppa, A., Gebremichael, M., Zambon, R.C., Yeh, W.W.G., and Hopson, T.M.: Seasonal Hydropower Planning for  
583 Data-Scarce Regions Using Multimodel Ensemble Forecasts, Remote Sensing Data, and Stochastic Programming.  
584 *WATER RESOURCES RESEARCH*, 55(11), 8583-8607, DOI: 10.1029/2019WR025228, 2019.

585

586 Lehner, B., and 14 coauthors: High-resolution mapping of the world's reservoirs and dams for sustainable river-flow  
587 management. *Frontiers in Ecology and the Environment* 9 (9): 494-502, 2011

588 Lehner, B., Verdin, K., Jarvis, A.: New global hydrography derived from spaceborne elevation data. *Eos, Transactions,*  
589 *AGU*, 89(10): 93-94, 2008

590 Lien, G. Y., Kalnay, E., Miyoshi, T., and Huffman, G. J.: Statistical properties of global precipitation in the NCEP  
591 GFS model and TMPA observations for data assimilation. *Monthly Weather Review*, 144(2), 663–679, doi:  
592 10.1175/MWR-D-15-0150.1, 2016.

593 Maranan, M., Fink, A. H., Knippertz, P., Amekudzi, L. K., Atiah, W. A., and Stengel, M.: A process-based validation  
594 of GPM IMERG and its sources using a mesoscale rain gauge network in the West African forest zone. *Journal of*  
595 *Hydrometeorology*, 21(4), 729-749, 2020

596 Mase, A. S., and Prokopy, L.S.: Unrealized Potential: A review of perceptions and use of weather and climate infor-  
597 mation in agricultural decision making. *Weather Climate and Society* 6(1):47-61. DOI: 10.1175/Wcas-D-12-00062.1,  
598 2014.

599 Mlawer, E. J., Taubman, S. J., Brown, P. D., Iacono, M. J., and Clough, S. A.: Radiative transfer for inhomogeneous  
600 atmospheres: RRTM, a validated correlated-k model for the longwave. *Journal of Geophysical Research:*  
601 *Atmospheres*, 102(D14), 16663-16682, 1997.

602 National Centers for Environmental Prediction.: National Centers for Environmental Prediction: The Global Forecast  
603 System (GFS) -Global Spectral Model (GSM). Retrieved from  
604 [https://www.emc.ncep.noaa.gov/emc/pages/numerical\\_forecast\\_systems/gfs/documentation.php](https://www.emc.ncep.noaa.gov/emc/pages/numerical_forecast_systems/gfs/documentation.php), last access: Sep  
605 2021, 2021a

606 National Centers for Environmental Prediction.: National Centers for Environmental Prediction: FV3: The GFDL  
607 Finite-Volume Cubed-Sphere Dynamical Core, Retrieved from <https://www.gfdl.noaa.gov/fv3/>, last access: Sep 2021,  
608 2021b

609 National Centers for Environmental Prediction/National Weather Service/NOAA/U.S. Department of Commerce.:  
610 NCEP GFS 0.25 Degree Global Forecast Grids Historical Archive, doi:10.5065/D65D8PW, 2015

611 Pandya, R., Hodgson, A., Hayden, M.H., Akweongo, P., Hopson, T., Forgor, A.A., Yoksas, T., Dalaba, M.A., Dukic,  
612 V., Mera, R., and Dumont, A., McCormack, K., Anaseba, D., Awine, T., Boehnert, J., Nyaaba, G., Laing, A., and  
613 Semazzi, F.: Using weather forecasts to help manage meningitis in the West African Sahel. *Bulletin of the American*  
614 *Meteorological Society* 96(1):103-+. doi: 10.1175/Bams-D-13-00121.1, 2015

615 Patt, A. G., Ogallo, L., and Hellmuth, M.: Sustainability—Learning from 10 years of climate outlook forums in Africa.  
616 *Science* 318(5847):49-50. doi:10.1126/science.1147909, 2007.

617 Pirret, J. S., Daron, J. D., Bett, P. E., Fournier, N., and Foamouhoue, A. K.: Assessing the skill and reliability of  
618 seasonal climate forecasts in Sahelian West Africa. *Weather and Forecasting*, 35(3), 1035-1050, doi:10.1175/WAF-  
619 D-19-0168.1, 2020.

620 Roudier, P., Alhassane, A., Baron, C., Louvet, S., and Sultan, B.: Assessing the benefits of weather and seasonal  
621 forecasts to millet growers in Niger. *Agricultural and forest meteorology*, 223, 168-180, doi:  
622 10.1016/j.agrformet.2016.04.010, 2016.

623 Saha, S., Moorthi, S., Wu, X., Wang, J., Nadiga, S., Tripp, P., Behringer, D., Hou, Y.-T., Chuang, H.-Y., Iredell, M.,  
624 Ek, M., Meng, J., Yang, R., Mendez, M.P., van den Dool, H., Zhang, Q., Wang, W., Chen, M., and Becker, E.: The  
625 NCEP climate forecast system version 2. *Journal of climate*, 27(6), 2185-2208, doi:10.1175/JCLI-D-12-00823.1,  
626 2014.

627 Satgé, F., Defrance, D., Sultan, B., Bonnet, M. P., Seyler, F., Rouché, N., and Paturel, J. E.: Evaluation of 23 gridded  
628 precipitation datasets across West Africa. *Journal of Hydrology*, 581, 124412, doi:10.1016/j.jhydrol.2019.124412 ,  
629 2020.

630 Sorí, R., Nieto, R., Drumond, A., and Gimeno, L.: The Niger River Basin Moisture Sources: A Lagrangian  
631 Analysis. *Atmosphere*, 8(2), 38, doi: 10.3390/atmos8020038, 2017.

632 Sridevi, C., Singh, K. K., Suneetha, P., Durai, V. R., and Kumar, A.: Rainfall forecast skill of Global Forecasting  
633 System (GFS) model over India during summer monsoon 2015. *Geofizika*, 35(1), 39–52, doi: 10.15233/gfz.2018.35.4,  
634 2018.

635 Sylla, M. B., Faye, A., Giorgi, F., Diedhiou, A., and Kunstmann, H.: Projected heat stress under 1.5 C and 2 C global  
636 warming scenarios creates unprecedented discomfort for humans in West Africa. *Earth's Future*, 6(7), 1029-1044, doi:  
637 10.1029/2018EF000873, 2018.

638 Tian, D., Wood, E.F., and Yuan, X.: CFSv2-based sub-seasonal precipitation and temperature forecast skill over the  
639 contiguous United States. *Hydrology and Earth System Sciences*, 21, 1477–1490, doi:10.5194/hess-21-1477-2017,  
640 2017.

641 Towner, J., Cloke, H.I., Zsoter, E., Flamig, Z., Hoch, J.M., Bazo, J., de Perez, E.C., and Stephens, E.M.: Assessing  
642 the performance of global hydrological models for capturing peak river flows in the Amazon basin. *Hydrology and*  
643 *Earth System Sciences*, 23, 3057–3080, doi:10.5194/hess-23-3057-2019, 2019.

644 van de Giesen, N., Hut, R., & Selker, J.: The trans-African hydro-meteorological observatory (TAHMO). *Wiley*  
645 *Interdisciplinary Reviews: Water*, 1(4), 341-348, doi:10.1002/wat2.1034, 2014

646 Wang, J. W. A., Sardeshmukh, P. D., Compo, G. P., Whitaker, J. S., Slivinski, L. C., McColl, C. M., and Pegion, P.  
647 J.: Sensitivities of the NCEP global forecast system. *Monthly Weather Review*, 147(4), 1237–1256, doi:  
648 10.1175/MWR-D-18-0239.1, 2019.

649 Yuan, X., E. F. Wood, and M. Liang: Integrating weather and climate prediction: toward seamless hydrologic  
650 forecasting. *Geophysical Research Letters*, 41, 5891–5896, doi:10.1002/2014GL061076, 2914.

651 Zhang, C., Xue, M., Supinie, T. A., Kong, F., Snook, N., Thomas, K. W., Brewster, K., Jung, Y., Harris, L.M. and  
652 Lin, S. J.: How well does an FV3-based model predict precipitation at a convection-allowing resolution? Results from  
653 CAPS forecasts for the 2018 NOAA hazardous weather test bed with different physics combinations. *Geophysical*  
654 *Research Letters*, 46(6), 3523-3531, doi:10.1029/2018GL081702, 2019.

655